AGU ADVANCING EARTH AND SPACE SCIENCES

Geophysical Research Letters

RESEARCH LETTER
10.1029/2024GL108335

Revisiting Winter Southern Ocean CO_2 Uptake Based on CALIPSO Observations

Hao Huang[1], Ke Zhang[1], Zhaoru Zhang[2], Walker Smith Jr.[2], Jianfeng He[3], Na Liu[4], and Chengfeng Le[1]

[1]Ocean College, Zhejiang University, Zhejiang, China, [2]School of Oceanography, Shanghai Jiao Tong University, Shanghai, China, [3]Polar Research Institute of China, Shanghai, China, [4]Norwegian Research Center NORCE, Bergen, Norway

Key Points:

- A new method was proposed to reconstruct pressure of CO_2 (pCO$_2$) using CALIPSO-derived b_{bp} data
- A 16-year Cloud-Aerosol Lidar and Infrared Pathfinder Satellite Observation observation-based pCO$_2$ product was constructed
- The CO_2 uptake capacity in the Southern Ocean during winter was estimated

Supporting Information:

Supporting Information may be found in the online version of this article.

Correspondence to:

C. Le,
chengfengle@zju.edu.cn

Citation:

Huang, H., Zhang, K., Zhang, Z., Smith, W., Jr., He, J., Liu, N., & Le, C. (2024). Revisiting winter Southern Ocean CO_2 uptake based on CALIPSO observations. *Geophysical Research Letters*, *51*, e2024GL108335. https://doi.org/10.1029/2024GL108335

Received 19 JAN 2024
Accepted 23 MAY 2024

Abstract The absorption of atmospheric carbon dioxide (CO_2) in the Southern Ocean represents a critical component of the global oceanic carbon budget. Previous assessments of air-sea carbon flux variations and long-term trends in polar regions during winter have faced limitations due to scarce field data and the lack of ocean color satellite imagery, causing uncertainties in estimating CO_2 flux estimation. This study utilized the Cloud-Aerosol Lidar and Infrared Pathfinder Satellite Observation satellite to construct a continuous 16-year (2006–2021) time series of sea surface partial pressure of CO_2 (pCO$_2$) in the Southern Ocean. Our findings revealed that the polar region in South Ocean acts as a carbon sink in winter, with CO_2 flux of ~30 TgC in high-latitude areas (South of 50°S). This work highlights the efficacy of active remote sensing for monitoring sea surface pCO$_2$ and contributes insights into the dynamic carbonate systems of the Southern Ocean.

Plain Language Summary Climate change data from recent decades have consistently shown an increase in atmospheric CO_2 concentration. The Southern Ocean, a major carbon sink, is critical in this regard. However, limitations in ocean color remote sensing and infrequent sampling hinder a complete understanding of carbon uptake in high-latitude regions during winter. Previous reconstructions inadequately considered the biological effect on the air-sea CO_2 exchange process in winter. This study used observations from an active remote sensing satellite to represent the biological effects of CO_2 and construct a long-term time series of sea surface CO_2 level for the Southern Ocean. Additionally, the study reassessed the CO_2 uptake capacity of the Southern Ocean in winter. These findings suggest that previous estimates may underestimate the CO_2 uptake capacity in the high-latitude regions during winter, potentially due to underestimations of biological effects. This research underscores the value of active remote sensing for obtaining critical biogeochemical parameters in high-latitude oceans, providing an essential tool for monitoring carbonate systems.

1. Introduction

The Southern Ocean, constituting a quarter of the global ocean surface area, absorbs 40% of anthropogenic carbon emissions (Friedlingstein et al., 2022; Khatiwala et al., 2013). The region functions as a crucial carbon sink within the global ocean, playing a significant role in the exchange of carbon between the ocean and the atmosphere. Therefore, understanding the Southern Ocean carbon sink and its variability is critical for climate assessments and the global carbon budget. However, achieving precise quantification of air-sea CO_2 fluxes remains challenging due to historical undersampling in these harsh and remote regions. Traditionally, estimation of air-sea CO_2 fluxes in the Southern Ocean heavily relies on ship-based measurements of surface pCO$_2$. This method suffers from limited spatial coverage and seasonal bias due to poor sampling during stormy autumn and winter periods (Bakker et al., 2016; Ritter et al., 2017; Rödenbeck et al., 2015; Sutton et al., 2021). These limitations hinder a comprehensive understanding of air-sea CO_2 exchange in the Southern Ocean. To address this issue, numerous studies have attempted to fill the gap in pCO$_2$ data using different approaches, including observation-based interpolation (Gray et al., 2018; Mackay & Watson, 2021), biogeochemical process-based modeling (Lenton et al., 2013; Mongwe et al., 2016; Takao et al., 2020), and satellite-based derivation (Bennington et al., 2022; Landschützer et al., 2016) in the Southern Ocean. However, significant discrepancies persist in the CO_2 flux estimates derived from models, observation-based data products, and direct observations in the Southern Ocean, particularly in high-latitude regions with extremely low observation frequencies (Mackay & Watson, 2021; Prend et al., 2022; Wu & Qi, 2023).

Among these approaches, the satellite observation-based method involves integrating ship-based measured pCO_2 data with satellite-observed oceanic physical and biological variables, offering advantages in estimating sea surface pCO_2 in the global ocean. Various global sea surface pCO_2 products, including CSIR-ML6 (Gregor et al., 2019), LSCE-FFNN (Denvil-Sommer et al., 2019), MPI-SOMFFN (Landschützer et al., 2014, 2020) and JMA-MLR (Iida et al., 2021), have been generated from satellite-based observations. These products utilize satellite-observed chlorophyll-a (Chl-a) in conjunction with other physical parameters, such as sea surface temperature (SST), mixed layer depth (MLD), sea surface salinity (SSS), and atmospheric CO_2 (xCO_2), to reconstruct global sea surface pCO_2. These satellite-based products have provided valuable insights into variations in global carbon reserves. However, one assumption made in these reconstruction of sea surface pCO_2 in winter creates a substantial uncertainty. Satellite Chl-a measurements are extremely limited in the Southern Ocean during winter due to high solar zenith angles, cloud cover, and thick aerosols. To address this limitation, these products either assume a low Chl-a value (e.g., Chl-a = 0.1 mg m^{-3}) (Denvil-Sommer et al., 2019; Gregor et al., 2019) or rely solely on physical variables (Iida et al., 2021; Landschützer et al., 2014) to estimate winter pCO_2. This assumption neglects the influence of biological processes on pCO_2 during winter and may lead to an overestimation of sea surface pCO_2, consequently underestimating the air-sea CO_2 flux in the Southern Ocean.

The Cloud-Aerosol Lidar and Infrared Pathfinder Satellite Observation satellite can observe the Earth's surface under challenging lighting conditions, such as aerosols, thin clouds, and low solar angles (Lu et al., 2014; Winker et al., 2009). This capability enables the observation of the ocean surface at high latitudes during winter. The particulate backscatter coefficient (b_{bp}) derived from CALIPSO can serve as a proxy for phytoplankton biomass in high-latitude oceans when satellite color observations are unavailable (Behrenfeld et al., 2017, 2022). This enhances its ability to observe winter pCO_2 and carbon flux in high-latitude oceans (Zhang et al., 2022). Utilizing the strengths of the CALIPSO satellite in the Southern Ocean, we combined this information with other variables, including MLD, SST, SSS, wind and xCO_2, to develop a machine learning-based approach. This approach allowed us to generate a 16-year (2006–2021) time series of regional sea surface pCO_2 products in the Southern Ocean. Furthermore, we investigated the distribution and variation in air-sea CO_2 fluxes during winter. Our findings revealed that the high-latitude Southern Ocean acts as an CO_2 sink during winter, which differs from previous findings that suggested it is a CO_2 source.

2. Materials and Methods

2.1. Study Area

This study centers its attention on the Southern Ocean, specifically the region located south of 35°S. Based on Fay & McKinley, 2014, the Southern Ocean can be broadly categorized into four distinct biomes: the subtropical permanently stratified biome (STPS), the subtropical seasonally stratified biome (STSS), the subpolar seasonally stratified biome (SPSS), and the ice biome (ICE; Figure 1a). The STPS and the STSS regions possess relatively extensive coverage of remote sensing data, enabling a more detailed representation of carbon sequestration and carbon exchange trends. Conversely, the SPSS and ICE regions that constitute nearly one-third of the Southern Ocean play a significant role in the uptake of anthropogenic carbon (Khatiwala et al., 2009). However, this region experiences seasonal ice coverage and high solar zenith angles, resulting in the unavailability of Chl-a products from satellite observations (Figure 1c). This limitation introduces uncertainty when assessing carbon sequestration trends using a satellite-based observational approach. In this study during the analysis of the spatial and temporal distribution of pCO_2 and carbon flux in the subsequent sections, we categorize the STPS and STSS as low-latitude Southern Oceans and designate the SPSS and ICE as high-latitude Southern Oceans.

2.2. Data Sets

Ship-based measurements of pCO_2 were retrieved from the Surface Ocean CO_2 Atlas data base (SOCAT V2023) (Bakker et al., 2016). The SOCAT V2023 data set includes data from a total of 860 cruises conducted in the Southern Ocean from June 2006 to December 2021, resulting in an extensive data set comprising 5,602,672 data points. Note that only the data quality level classified as A to D was used in this study (QC_Flag = A~D) (Figure 1b).

The monthly CALIPSO-derived b_{bp} data from June 2006 to December 2021 were obtained from Lu et al. (2021). We mapped the monthly daytime and nighttime b_{bp} onto a 0.25° × 0.25° grid using a 2D linear interpolation

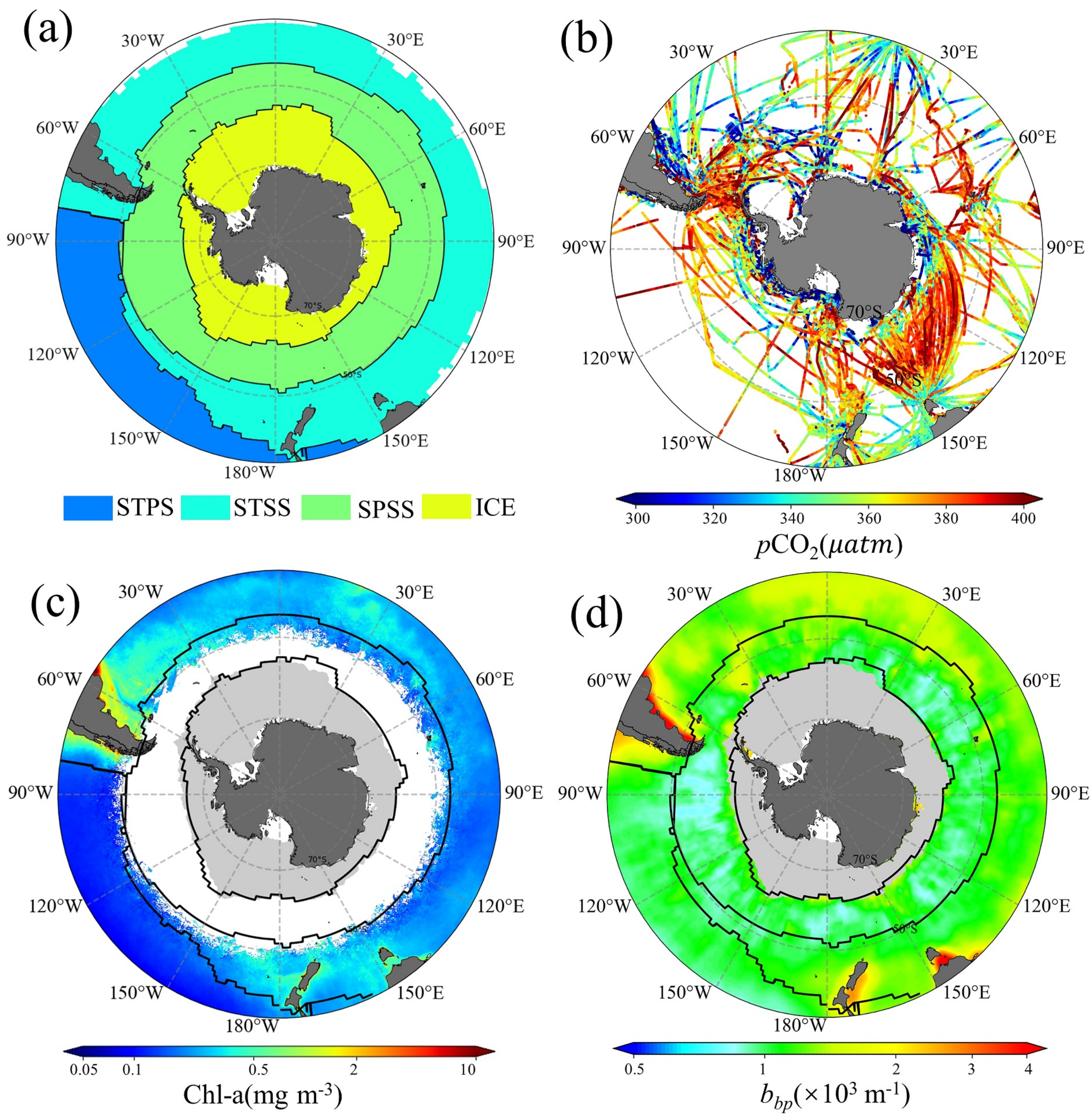

Figure 1. (a) Map of biomes defined by Fay and McKinley (2014). (b) Measured pCO_2 distributions in SOCAT v2023 (Bakker et al., 2016) for 2006–2021. (c) The mean winter (May, June, and July) Chl-a concentration from Moderate Resolution Imaging Spectroradiometer (2006–2021) (OBPG, 2018). (d) The mean winter (May, June, and July) b_{bp} derived through linear interpolation (2006–2021).

method. This approach, in contrast to the Chl-a product observed by the Moderate Resolution Imaging Spectroradiometer (Figure 1c), effectively covered the subpolar region during winter (Figure 1d).

Various environmental variables were acquired from different sources to estimate the Southern Ocean pCO_2. Monthly 9 km MW_IR OI SST are produced by Remote Sensing Systems (RSS, 2022). Monthly MLD (0.083° × 0.083°) were sourced from HYCOM (Behrenfeld et al., 2016). SSS (0.083° × 0.083°) were extracted from the GLORYS12V1 product of Copernicus Marine Global Reanalysis Product (Lellouche et al., 2018). Monthly wind data were sourced from the high-resolution Cross-Calibrated Multi-Platform data set (Mears et al., 2022). xCO_2 data were retrieved from the NOAA Marine Boundary Layer dry air mixing ratio of atmospheric CO_2 (Lan et al., 2023). Ice data were obtained from the AVHRR Pathfinder version 5.3 level 3 product (Saha et al., 2018).

2.3. $p\mathrm{CO_2}$ Retrieval and Evaluation

The machine learning-based Random Forest (RF) algorithm was used to predict $p\mathrm{CO_2}$ via b_{bp} and other environmental factors in the Southern Ocean followed the approach proposed in Tu et al. (2021). It establishes a nonlinear function between the target variable $p\mathrm{CO_2}$ and the input variables b_{bp}, SST, SSS, MLD, Wind, and $x\mathrm{CO_2}$:

$$p\mathrm{CO_2} = f(b_{bp}, \mathrm{SST}, SSS, \mathrm{MLD}, \mathrm{Wind}, x\mathrm{CO_2}) \tag{1}$$

To ensure compatibility with the CALIPSO-derived b_{bp} data, the input environmental variables were resampled to a 0.25° × 0.25°. Monthly environmental variables were employed for matching field measurements, thereby increasing the likelihood of obtaining cloud-free satellite pixels and increasing the number of matches. Prior to the matching process, the ship-based measured $p\mathrm{CO_2}$ data were averaged at approximately 25 km (0.25° × 0.25°) to align with the spatial resolutions of the predicted variables. The specific matching process adhered to the methodology of Le et al. (2019). Finally, a total of 140,787 matched pairs involving field-measured sea surface $p\mathrm{CO_2}$ and predicted variables from 860 cruises conducted between 2006 and 2021 were determined for the development of the $p\mathrm{CO_2}$ model.

To better assess the performance and robustness of the RF model in predicting $p\mathrm{CO_2}$, the satellite-field match up data set were divided into training data set and independent validation data set. Randomly selected field measured $p\mathrm{CO_2}$ from 80 cruises, amounting to approximately 12,362 data records, were used as independent validation data set and excluded from model calibration. The remaining portion was used to calibrate the RF model and further divided into two parts, with 70% for model training and 30% for crossing validation following previous studies (Chen et al., 2019; Tu et al., 2021). Various statistical metrics, including the correlation coefficient (R^2), root mean square error (RMSE), mean absolute error (MAE), and mean bias (MB) were utilized to evaluate the model's performance (Le et al., 2019; Tu et al., 2021). The error (±means standard deviation) is used when analyzing interannual variation (Le et al., 2019).

2.4. Candidate $p\mathrm{CO_2}$ Products for Comparison

Four globally applied sea surface $p\mathrm{CO_2}$ products, each generated through distinct methodologies, were selected for comparative analysis of $\mathrm{CO_2}$ flux variations in the Southern Ocean. These products include LSCE-FFNN (Denvil-Sommer et al., 2019), MPI-SOMFFN (Landschützer et al., 2014, 2020), CSIR-ML6 (Gregor et al., 2019), and JMA-MLR (Iida et al., 2021). All these products are derived from SOCAT $p\mathrm{CO_2}$ data and satellite-based observations utilizing machine learning approaches (Table S1 in Supporting Information S1). Among these four products, the CSIR-ML6 and LSCE-FFNN products employed low-concentration values (log(Chl-a) = 0 mg m^{-3}) to fill in missing Chl-a data in high-latitude regions during winter. In contrast, the MPI-SOMFFN and JMA-MLR products did not include the Chl-a variable during the calculation of the global sea surface $p\mathrm{CO_2}$ in winter. Due to variations in the data used and diverse strategies for handling ice concentration in different products, the updated $p\mathrm{CO_2}$ data provided in Fay et al. (2021) was used to calculate air-sea $\mathrm{CO_2}$ flux to ensure comparability of the final results. The bulk sea-air $\mathrm{CO_2}$ flux is commonly calculated according to Garbe et al. (2014). Note that the field measured $p\mathrm{CO_2}$ in STPS regions is extremely scarceness (Figure 1b), which may cause high uncertainty in $p\mathrm{CO_2}$ retrieval product, this region was excluded during calculating the monthly and annual regional mean $p\mathrm{CO_2}$ and sea-air $\mathrm{CO_2}$ flux for the low latitude region.

3. Result

3.1. Model Performance

The performance of the RF model in estimating sea surface $p\mathrm{CO_2}$ in the Southern Ocean utilizing CALIPSO-based b_{bp} data closely aligned with the observed values (Figure 2). Throughout the model training process, the RF model exhibited exceptional performance, indicating that the model has a high level of robustness. The RF model yielded a RMSE of 6.2 µatm, a MAE of 3.4 µatm, a MB of 0.07 µatm and a R^2 value of 0.99 for the training data set, and yielded a RMSE of 16.3 µatm, a MAE of 9.0 µatm, a MB of 0.09 µatm and a R^2 value of 0.83 for the cross-validation data set. Although the performance of the model degraded for the independent validation data set, yielding a RMSE of 17.3 µatm, a MAE of 12.9 µatm, a MB of 0.15 µatm and a R^2 value of 0.56, it successfully replicated variation of field measured $p\mathrm{CO_2}$ (Figure 2d). Since other products did not provide specific

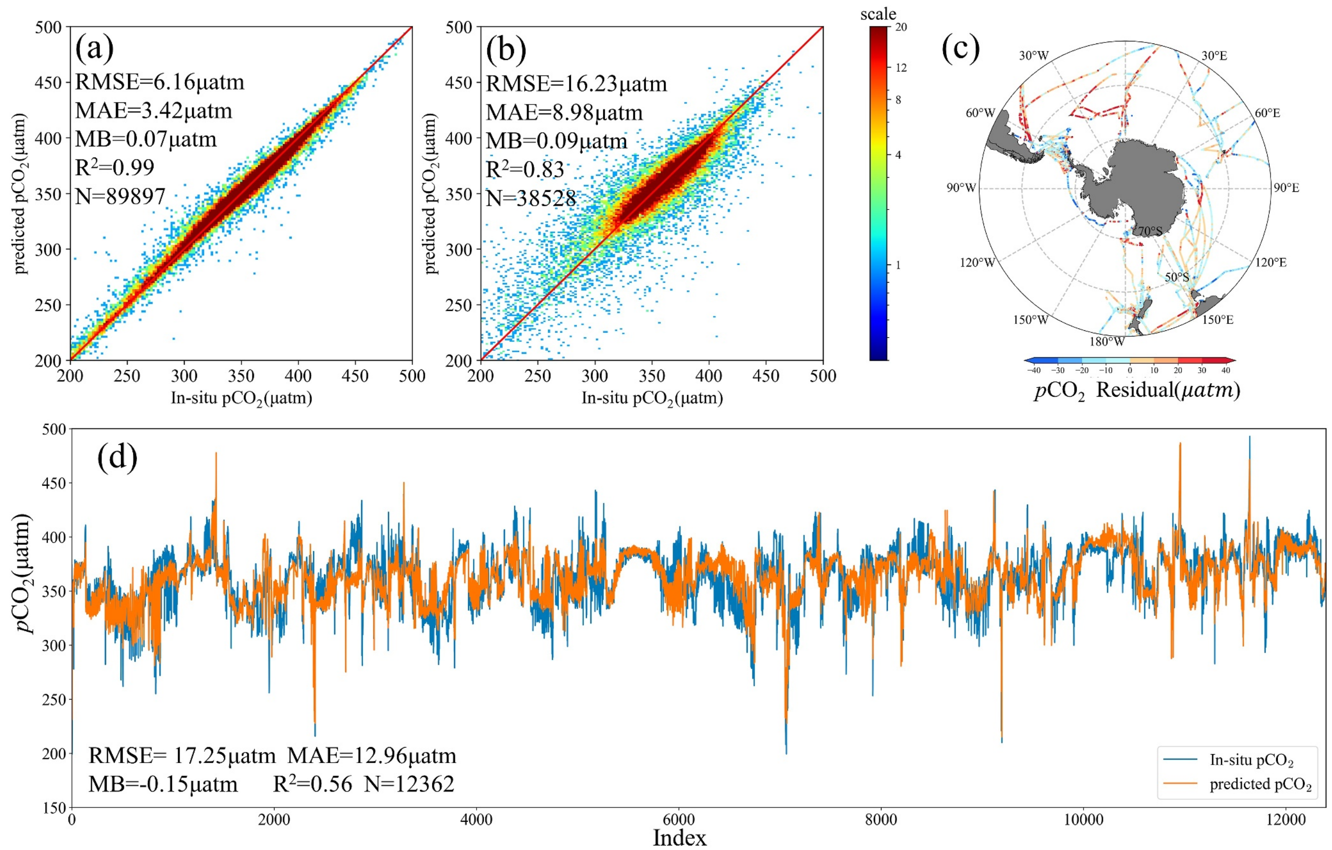

Figure 2. The performance of the Random Forest (RF) model in estimating sea surface pCO_2 during (a) model training and (b) cross-validation phase. (c) Distribution of pCO_2 residual refers to the discrepancy between predicted and measured values for the independent randomly selected 80 cruises. (d) Comparison between in-situ pCO_2 and pCO_2 predicted by the RF model for the 80 randomly selected cruises.

performance data within the Southern Ocean, their accuracy was also evaluated using the same data set of 80 randomly selected cruise pCO_2 measurements in this study. The results indicated that the pCO_2 values derived from CALIPSO-based observations exhibited comparable performance to those of the four products (Figure S1 and Table S2 in Supporting Information S1), with RMSE values of approximately 18.0 μatm, MAE values of approximately 13.0 μatm, MB values of ±1.0 μatm and R^2 values of ~0.55. Given the large variation range of pCO_2 in the South Ocean (~200–450 μatm), these findings suggest that the pCO_2 data derived from CALIPSO-based observations can be effectively utilized to investigate the spatial and temporal variations in CO_2 uptake in the Southern Ocean.

3.2. Variations in Sea Surface pCO_2

All five pCO_2 products consistently revealed similar spatial distributions and temporal fluctuations (Figure S2 in Supporting Information S1 and Figure 3a). In broad terms, the low-latitude region, situated between 35°S and 50°S, exhibited lower pCO_2 values than the high-latitude regions, primarily attributed to the presence of greater phytoplankton biomass (Figure S2 in Supporting Information S1). Seasonal variations were evident, with pCO_2 values being lower in the summer months and higher in winter (Figure 3a). Notably, the CALIPSO-based product exhibited a discernible increasing trend characterized by an annual increase rate of 1.63 ($R^2 = 0.92$, $P < 0.001$) μatm year^{-1}, which closely aligns with the trends observed in the other four products (Table S3 in Supporting Information S1). Importantly, this increase rate was found to be lower than that of atmospheric CO_2, (2.23 μatm year^{-1}), implying a growing annual carbon uptake in the Southern Ocean from 2006 to 2021. However, a notable distinction emerged in the magnitude of sea surface pCO_2 among the five pCO_2 products, and this difference exhibited regional variation. In the low-latitude region (Figure 3b), the disparity primarily manifested during summer, with CALIPSO-derived pCO_2 values being lower than those of the other four products. In

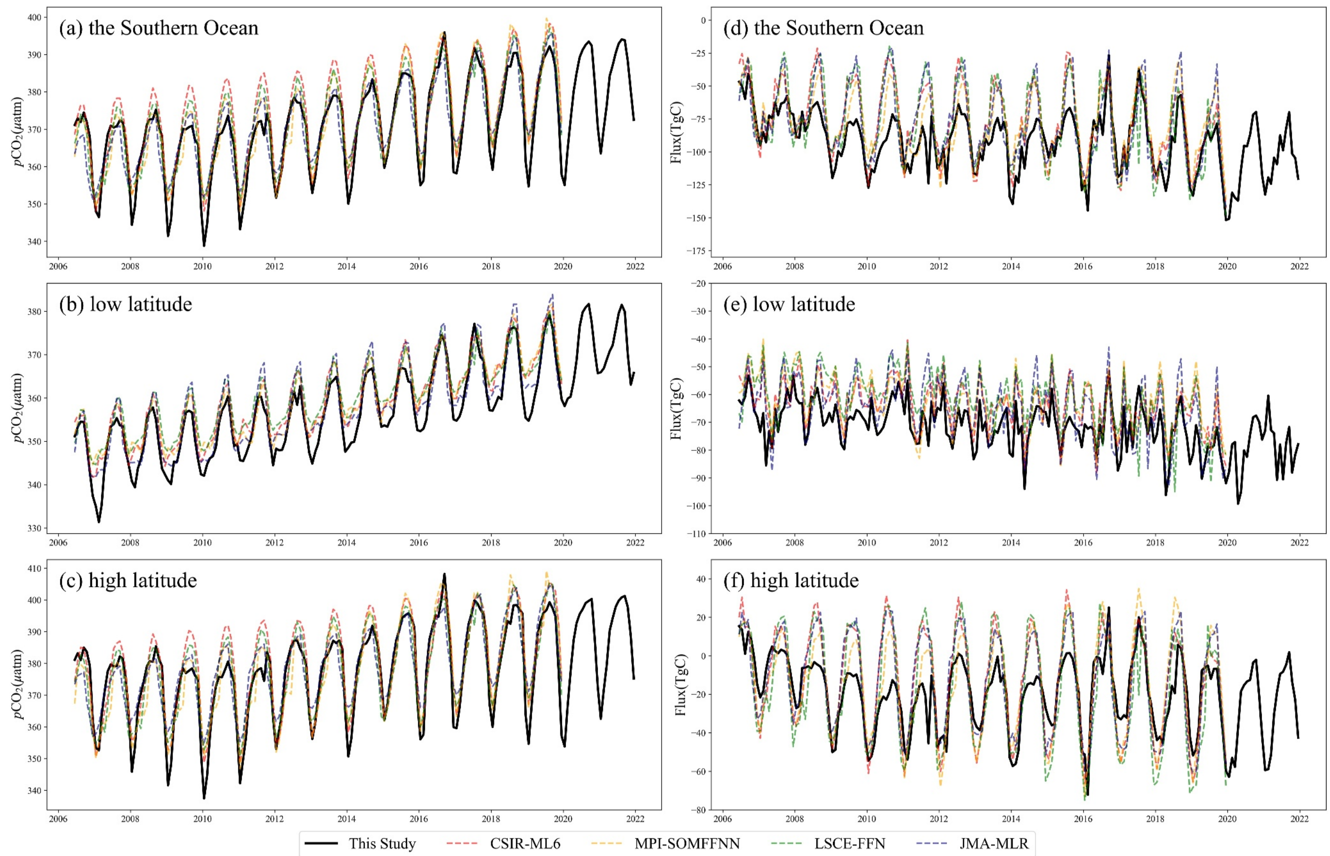

Figure 3. The time series of regional pCO_2 (a–c) and sea–air CO_2 flux (d–f) for the period 2006–2021. (a, d) For the entire Southern Ocean and (b, e), (c, f) for the low- and high-latitude areas, respectively. Note that the regional mean for low-latitude was only calculated from the subtropical seasonally stratified biome region.

contrast, within the high-latitude region, the difference was more prominent during winter (Figure 3c). During winter and early spring, the pCO_2 data derived from CALIPSO consistently displayed lower values than those derived from the other four products and remained consistently below atmospheric CO_2 levels. This suggests that these regions function as a carbon sink during winter. Conversely, the other products had pCO_2 levels higher than the atmospheric CO_2 level, indicating carbon sources during the winter months.

3.3. Sea–Air CO_2 Flux Variability

The assessment of the Southern Ocean's CO_2 uptake capacity was analyzed by calculating the air-sea CO_2 flux using the CALIPSO-based pCO_2 product. The results demonstrated that the CALIPSO-based air-sea CO_2 fluxes exhibited spatial and temporal distributions comparable to those estimated from the other four products (Figure S3 in Supporting Information S1 and Figure 3d). Across all products, it was evident that the Southern Ocean acted as a robust carbon sink from 2006 to 2021 (Figure 3d and Table S3 in Supporting Information S1). The CALIPSO-based product yielded the highest annual mean air-sea CO_2 flux, with a value of -1.12 ± 0.12 Pg C year^{-1} in the Southern Ocean. However, it also exhibited the lower rate of increase, with an estimated increase rate of 0.018 Pg C year^{-1} ($R^2 = 0.43$, $p < 0.001$) in the Southern Ocean. The low-latitude region consistently demonstrated a strong and stable carbon uptake capacity throughout the year, absorbing ~0.86 ± 0.08 Pg C year^{-1}. This value significantly exceeded the carbon uptake of approximately 0.25 ± 0.08 Pg C year^{-1} estimated for the high-latitude regions based on the CALIPSO-based product.

Among the five products, the air-sea CO_2 fluxes exhibited minor differences in the low-latitude region (Figure 3e). However, noticeable disparities were observed in the high-latitude region during the winter months (Figure 3f). The CALIPSO-based product consistently indicated a greater carbon flux than did the other four products during winter, revealing a previously unrecognized overall carbon sink. Figure 4 provides a summary of

10.1029/2024GL108335

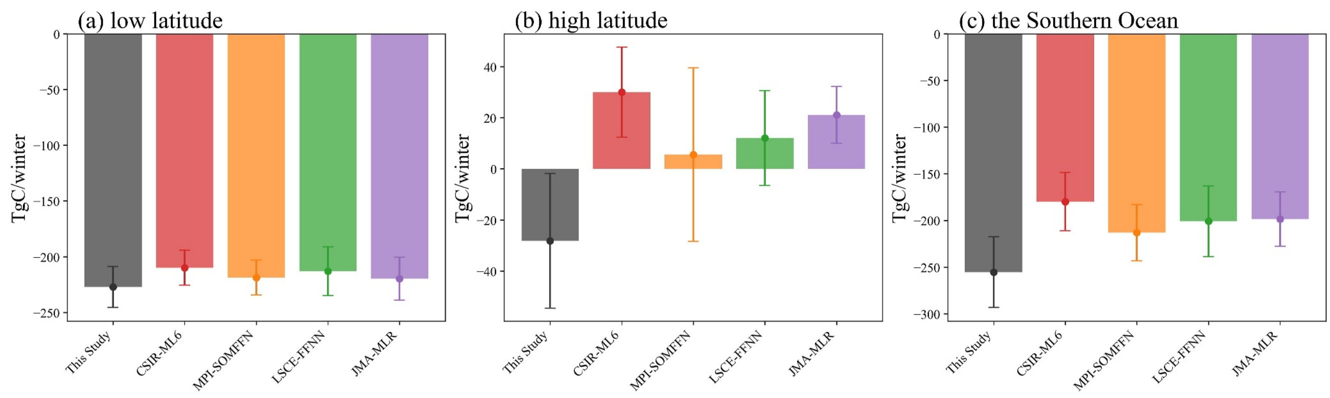

Figure 4. Comparison of regional mean winter (May, June, and July) air-sea CO_2 flux of different products in the low-latitude region (a), and the high latitude region (b), and the Southern Ocean.

the climatological air-sea CO_2 flux budget in the Southern Ocean, estimated from different pCO_2 products for the winter season. Due to missing Chl-a data occurring primarily in May, June, and July (Figure S4 in Supporting Information S1), the carbon fluxes in these 3 months were averaged to establish the austral winter climatology for comparison. All five products yielded comparable climatological winter air-sea CO_2 flux values for the low-latitude region (Figure 4a), however, the CALIPSO-based product revealed a significantly greater CO_2 uptake capacity in the high-latitude region during winter (Figure 4b), with a climatological winter air-sea CO_2 flux of −28.2 ± 26.3 Tg C. In contrast, the CSIR-ML6, MPI-SOMFFN, LSCE-FFNN, and JMA-MLR products all portrayed this area as a CO_2 source, with climatological winter air-sea CO_2 flux values of 30.1 ± 17.64, 5.6 ± 33.4, 12.1 ± 18.6 and 21.2 ± 11.1 TgC, respectively. As a result, the CALIPSO-based product yielded higher CO_2 uptake value than the other four products for the entire South Ocean (Figure 4c), with value higher than 250 TgC in winter. These results suggest that the CO_2 uptake might be underestimated by pervious estimations in winter.

4. Discussion

Precisely assessing the carbon uptake capacity in the Southern Ocean presents notable challenges due to the vast expanse of this area and the scarcity of field measurements, particularly during winter when observational data are limited and ocean color products unavailable. Although various methodologies, such as model simulation (Kessler & Tjiputra, 2016; Mongwe et al., 2016, 2018), interpolation of measured data (Bushinsky et al., 2019; Landschützer et al., 2015; Rödenbeck et al., 2015), and inversion of remote sensing products (Gregor et al., 2017; Hauck et al., 2023), have been developed to acquire spatially and temporally continuous global pCO_2 data, applying these methods in the Southern Ocean during winter is challenging. Field measurements for high-latitude regions during winter are lacking due to severe environmental conditions, rendering interpolation methods inapplicable to these regions. Model simulation methods, although capable of identifying large-scale trends in the oceanic carbon cycle, are constrained in their ability to analyze complex variable relationships in specific regions, leading to discrepancies between simulations and measurements. Remote sensing data inversion methods aim to partially address these limitations; however, ocean color products are unavailable during winter, introducing uncertainties in pCO_2 products.

We used a novel approach based on CALIPSO observations to reconstruct pCO_2 levels, resulting in a long-term time series of pCO_2 data for the Southern Ocean. Different from other pCO_2 products reconstructed from ocean color observations (e.g., Chl-a), this approach utilized b_{bp} derived from CALIPSO as a proxy for phytoplankton biomass during winter. The viability of this approach was substantiated that established CALIPSO-derived b_{bp} as an optimal proxy for phytoplankton biomass when ocean color is unavailable (Behrenfeld et al., 2013). Additionally, a recent study demonstrated a strong relationship between CALIPSO b_{bp} and Chl-a in high-latitude oceans (Zhang et al., 2022). Independent evaluation of the CALIPSO-based pCO_2 product confirmed its ability to capture spatial and temporal variations in sea surface pCO_2 in the Southern Ocean (Figures 2c and 2d). Crucially, the b_{bp}-based approach exhibited comparable accuracy to that of other products based on ocean color observations when Chl-a data were available (Table S2 and Figure S1 in Supporting Information S1). In addition, we further evaluated the effect from the change of machine learning models on the constructed pCO_2 level, and found that the switch of construction approach does not significantly affect the pCO_2 time series in this study (data not shown). These indicate that differences between the pCO_2 concentration and air-sea carbon flux estimates derived from the CALIPSO-based product and ocean color satellite-based products are not attributable to uncertainties in the reconstruction approach.

Using the CALIPSO-derived pCO_2 products, we revisited the carbon uptake capacity in the Southern Ocean by calculating the air-sea CO_2 flux. Our results showed that the high latitude region in South Ocean acts as carbon sink during winter, which is contrast to the results from the other four products, revealing as a carbon source (Figure 4b). This divergence from most previous ocean color satellite observation-based products suggested that these earlier products may have neglected or underestimated initiate biological effects while overestimating pCO_2 in winter. Notably, phytoplankton blooms often in early winter (Arteaga et al., 2020; Uchida et al., 2019), contributing to this difference. The Southern Ocean Carbon and Climate Observations and Modeling project float data, for instance, identify the region south of the Antarctic Circumpolar Current (ACC) as a significant carbon source due to the influence of carbon-rich deep water (Bushinsky et al., 2019; Gray et al., 2018). Regional measurements by 9 aircraft projects suggested that the Southern Ocean is a relatively neutral carbon sink during winter (Long et al., 2021). Our findings differ primarily due to the regions considered for carbon flux calculations in our study, which focused on areas lacking the ocean color Chl-a product; these regions are considerably larger than the regions south of the ACC. The CALIPSO-based pCO_2 product indeed revealed a near-neutral or weak carbon source south of the ACC during winter.

In summary, our study highlights the advantages of utilizing active remote sensing satellites for observing sea surface pCO_2 and obtaining a better understanding of the carbon cycle in high-latitude oceans. However, we acknowledge the limitations of our study. Like many other approaches, the machine learning-based pCO_2 retrieval model is inherently empirical, and its performance relies heavily on the calibration data set. Given the limited field measurements in winter, significant uncertainty may exist during this season, emphasizing the need for additional winter field measurements in high-latitude regions to assess the accuracy of these reconstructed pCO_2 products. Moreover, the distribution of b_{bp} data exhibited distinctive features. While it serves as an effective means of addressing data gaps in high-latitude regions to some extent, the sampling of surface ocean properties is sparse compared to ocean color observations. Interpolation fills data gaps between adjacent trajectories, which may introduce uncertainty in the distribution of sea surface b_{bp}. Therefore, future research efforts should prioritize the development of more comprehensive data sources to increase the precision of monitoring CO_2 flux trends. Nonetheless, this study provides an alternative approach to deriving pCO_2 in high-latitude oceans during winter and offers valuable insights into the dynamics of CO_2 fluxes in the Southern Ocean. We recommend merging active remote sensing (e.g., Lidar) data with passive satellite observation data (e.g., ocean color) to improve the accuracy of quantifying regional and global ocean carbon fluxes in future studies.

Data Availability Statement

The SOCAT V2023 (Bakker et al., 2016) are available at https://www.ncei.noaa.gov/data/oceans/ncei/ocads/data/0278913/SOCATv2023_SouthernOceans.tsv, the CALIPSO-derived b_{bp} data (Lu et al., 2021) is from http://orca.science.oregonstate.edu/lidar.data.php. The sources of environmental variables are as follows: SST (RSS, 2022) via https://www.remss.com/measurements/sea-surface-temperature/oisst-description/, MLD (Behrenfeld et al., 2016) via http://orca.science.oregonstate.edu/1080.by.2160.monthly.hdf.mld125.hycom.php, SSS (Lellouche et al., 2018) via https://data.marine.copernicus.eu/product/GLOBAL_MULTIYEAR_PHY_001_030/description, wind (Mears et al., 2022) via https://data.remss.com/ccmp/, ice (Saha et al., 2018) via https://www.ncei.noaa.gov/access/metadata/landing-page/bin/iso?id=gov.noaa.nodc:AVHRR_Pathfinder-NCEI-L3C-v5.3, xCO_2 (Lan et al., 2023) via https://www.esrl.noaa.gov/gmd/ccgg/mbl/ and the sea level pressure (Kanamitsu et al., 2002) via https://psl.noaa.gov/data/gridded/data.ncep.reanalysis2.html. The source of the comparison products (Fay et al., 2021) is https://zenodo.org/records/8280457.

Acknowledgments
This work was supported by the National Natural Science Foundation of China (42325602, 41976164), National Key Research and Development Program of China (2022YFC2807601), and Natural Science Foundation of Zhejiang Province for Distinguished Young Scholars (LR20D060002). We extend our appreciation to all the data providers and the authors of the compared products mentioned in the article. We also thank the anonymous reviewers and editor for their constructive feedback, which has substantially enhanced the clarity and presentation of the manuscript.

References

Arteaga, L. A., Boss, E., Behrenfeld, M. J., Westberry, T. K., & Sarmiento, J. L. (2020). Seasonal modulation of phytoplankton biomass in the Southern Ocean. *Nature Communications*, *11*(1), 5364. https://doi.org/10.1038/s41467-020-19157-2

Bakker, D. C. E., Alin, S. R., Becker, M., Bittig, H. C., Castaño-Primo, R., Feely, R. A., et al. (2016). A multi-decade record of high-quality fCO_2 data in version 3 of the Surface Ocean CO_2 Atlas (SOCAT). *Earth System Science Data*, *8*(2), 383–413. https://doi.org/10.25921/1h9f-nb73

Behrenfeld, M. J., Hu, Y. X., Bisson, K. M., Lu, X. M., & Westberry, T. K. (2022). Retrieval of ocean optical and plankton properties with the satellite Cloud-Aerosol Lidar with Orthogonal Polarization (CALIOP) sensor: Background, data processing, and validation status. *Remote Sensing of Environment*, *281*, 113235. https://doi.org/10.1016/j.rse.2022.113235

Behrenfeld, M. J., Hu, Y. X., Hostetler, C. A., Dall'Olmo, G., Rodier, S. D., Hair, J. W., & Trepte, C. R. (2013). Space-based lidar measurements of global ocean carbon stocks. *Geophysical Research Letters*, *40*(16), 4355–4360. https://doi.org/10.1002/grl.50816

Behrenfeld, M. J., Hu, Y. X., O'Malley, R. T., Boss, E. S., Hostetler, C. A., Siegel, D. A., et al. (2017). Annual boom–bust cycles of polar phytoplankton biomass revealed by space-based lidar. *Nature Geoscience*, *10*(2), 118–122. https://doi.org/10.1038/ngeo2861

Behrenfeld, M. J., O'Malley, R. T., Boss, E. S., Westberry, T. K., Graff, J. R., Halsey, K. H., et al. (2016). Revaluating ocean warming impacts on global phytoplankton. *Nature Climate Change*, *6*(3), 323–330. https://doi.org/10.1038/nclimate2838

Bennington, V., Galjanic, T., & McKinley, G. A. (2022). Explicit physical knowledge in machine learning for ocean carbon flux reconstruction: The $p\mathrm{CO_2}$ residual method. *Journal of Advances in Modeling Earth Systems*, *14*(10), e2021MS002960. https://doi.org/10.1029/2021ms002960

Bushinsky, S. M., Landschützer, P., Rödenbeck, C., Gray, A. R., Baker, D., Mazloff, M. R., et al. (2019). Reassessing Southern Ocean air-sea CO_2 flux estimates with the addition of biogeochemical float observations. *Global Biogeochemical Cycles*, *33*(11), 1370–1388. https://doi.org/10.1029/2019gb006176

Chen, S., Hu, C., Barnes, B. B., Wanninkhof, R., Cai, W. J., Barbero, L., & Pierrot, D. (2019). A machine learning approach to estimate surface ocean $p\mathrm{CO_2}$ from satellite measurements. *Remote Sensing of Environment*, *228*, 203–226. https://doi.org/10.1016/j.rse.2019.04.019

Denvil-Sommer, A., Gehlen, M., Vrac, M., & Mejia, C. (2019). LSCE-FFNN-v1: A two-step neural network model for the reconstruction of surface ocean $p\mathrm{CO_2}$ over the global ocean. *Geoscientific Model Development*, *12*(5), 2091–2105. https://doi.org/10.5194/gmd-12-2091-2019

Fay, A. R., Gregor, L., Landschützer, P., McKinley, G. A., Gruber, N., Gehlen, M., et al. (2021). Harmonization of global surface ocean $p\mathrm{CO_2}$ mapped products and their flux calculations; an improved estimate of the ocean carbon sink. *Earth System Science Data Discussions*, *2021*, 1–32. https://doi.org/10.5194/essd-2021-16

Fay, A. R., & McKinley, G. A. (2014). Global open-ocean biomes: Mean and temporal variability. *Earth System Science Data*, *6*(2), 273–284. https://doi.org/10.5194/essd-6-273-2014

Friedlingstein, P., O'sullivan, M., Jones, M. W., Andrew, R. M., Gregor, L., Hauck, J., et al. (2022). Global carbon budget 2022. *Earth System Science Data*, *14*(11), 4811–4900. https://doi.org/10.5194/essd-14-4811-2022

Garbe, C. S., Rutgersson, A., Boutin, J., de Leeuw, G., Delille, B., Fairall, C. W., et al. (2014). Transfer across the air-sea interface. In *Ocean-atmosphere interactions of gases and particles* (pp. 55–112). https://doi.org/10.1007/978-3-642-25643-1_2

Gray, A. R., Johnson, K. S., Bushinsky, S. M., Riser, S. C., Russell, J. L., Talley, L. D., et al. (2018). Autonomous biogeochemical floats detect significant carbon dioxide outgassing in the high-latitude Southern Ocean. *Geophysical Research Letters*, *45*(17), 9049–9057. https://doi.org/10.1029/2018GL078013

Gregor, L., Kok, S., & Monteiro, P. (2017). Empirical methods for the estimation of Southern Ocean CO_2: Support vector and random forest regression. *Biogeosciences*, *14*(23), 5551–5569. https://doi.org/10.5194/bg-14-5551-2017

Gregor, L., Lebehot, A. D., Kok, S., & Scheel Monteiro, P. M. (2019). A comparative assessment of the uncertainties of global surface ocean CO_2 estimates using a machine-learning ensemble (CSIR-ML6 version 2019a) – Have we hit the wall? *Geoscientific Model Development*, *12*(12), 5113–5136. https://doi.org/10.5194/gmd-12-5113-2019

Hauck, J., Gregor, L., Nissen, C., Patara, L., Hague, M., Mongwe, P., et al. (2023). The Southern Ocean carbon cycle 1985–2018: Mean, seasonal cycle, trends, and storage. *Global Biogeochemical Cycles*, *37*(11), e2023GB007848. https://doi.org/10.1029/2023GB007848

Iida, Y., Takatani, Y., Kojima, A., & Ishii, M. (2021). Global trends of ocean CO_2 sink and ocean acidification: An observation-based reconstruction of surface ocean inorganic carbon variables. *Journal of Oceanography*, *77*(2), 323–358. https://doi.org/10.1007/s10872-020-00571-5

Kanamitsu, M., Ebisuzaki, W., Woollen, J., Yang, S. K., Hnilo, J. J., Fiorino, M., & Potter, G. L. (2002). NCEP–DOE AMIP-II Reanalysis (R-2). *Bulletin America Meteorology Social*, *83*(11), 1631–1644. https://doi.org/10.1175/BAMS-83-11-1631

Kessler, A., & Tjiputra, J. (2016). The Southern Ocean as a constraint to reduce uncertainty in future ocean carbon sinks. *Earth System Dynamics*, *7*(2), 295–312. https://doi.org/10.5194/esd-7-295-2016

Khatiwala, S., Primeau, F., & Hall, T. (2009). Reconstruction of the history of anthropogenic CO_2 concentrations in the ocean. *Nature*, *462*(7271), 346–349. https://doi.org/10.1038/nature08526

Khatiwala, S., Tanhua, T., Mikaloff Fletcher, S., Gerber, M., Doney, S. C., Graven, H. D., et al. (2013). Global ocean storage of anthropogenic carbon. *Biogeosciences*, *10*(4), 2169–2191. https://doi.org/10.5194/bg-10-2169-2013

Lan, X., Tans, P., & Thoning, K., & NOAA Global Monitoring Laboratory. (2023). NOAA Greenhouse Gas Marine Boundary Layer Reference - CO_2 [Dataset]. *NOAA GML*. https://doi.org/10.15138/DVNP-F961

Landschützer, P., Gruber, N., & Bakker, D. C. (2016). Decadal variations and trends of the global ocean carbon sink. *Global Biogeochemical Cycles*, *30*(10), 1396–1417. https://doi.org/10.1002/2015GB005359

Landschützer, P., Gruber, N., Bakker, D. C., Landschützer, P., Gruber, N., Bakker, D. C., et al. (2020). An observation-based global monthly gridded sea surface $p\mathrm{CO_2}$ product from 1982 onward and its monthly climatology, version 5.5. Technical Report. https://doi.org/10.7289/V5Z899N6

Landschützer, P., Gruber, N., Bakker, D. C., & Schuster, U. (2014). Recent variability of the global ocean carbon sink. *Global Biogeochemical Cycles*, *28*(9), 927–949. https://doi.org/10.1002/2014GB004853

Landschützer, P., Gruber, N., Haumann, F. A., Rödenbeck, C., Bakker, D. C., Van Heuven, S., et al. (2015). The reinvigoration of the Southern Ocean carbon sink. *Science*, *349*(6253), 1221–1224. https://doi.org/10.1126/science.aab2620

Le, C., Gao, Y., Cai, W. J., Lehrter, J. C., Bai, Y., & Jiang, Z. P. (2019). Estimating summer sea surface $p\mathrm{CO_2}$ on a river-dominated continental shelf using a satellite-based semi-mechanistic model. *Remote Sensing of Environment*, *225*, 115–126. https://doi.org/10.1016/j.rse.2019.02.023

Lellouche, J. M., Greiner, E., Le Galloudec, O., Garric, G., Regnier, C., Drevillon, M., et al. (2018). Recent updates to the Copernicus Marine Service global ocean monitoring and forecasting real-time 1/12° high-resolution system. *Ocean Science*, *14*(5), 1093–1126. https://doi.org/10.5194/os-14-1093-2018

Lenton, A., Tilbrook, B., Law, R. M., Bakker, D., Doney, S. C., Gruber, N., et al. (2013). Sea–air CO_2 fluxes in the Southern Ocean for the period 1990-2009. *Biogeosciences*, *10*(6), 4037–4054. https://doi.org/10.5194/bg-10-4037-2013

Long, M. C., Stephens, B. B., McKain, K., Sweeney, C., Keeling, R. F., Kort, E. A., et al. (2021). Strong Southern Ocean carbon uptake evident in airborne observations. *Science*, *374*(6572), 1275–1280. https://doi.org/10.1126/science.abi4355

Lu, X., Hu, Y., Trepte, C., Zeng, S., & Churnside, J. H. (2014). Ocean subsurface studies with the CALIPSO spaceborne lidar. *Journal of Geophysical Research: Oceans*, *119*(7), 4305–4317. https://doi.org/10.1002/2014JC009970

Lu, X., Hu, Y., Yang, Y., Neumann, T., Omar, A., Baize, R., et al. (2021). New ocean subsurface optical properties from space lidars: CALIOP/CALIPSO and ATLAS/ICESat-2. *Earth and Space Science*, *8*(10), e2021EA001839. https://doi.org/10.1029/2021EA001839

Mackay, N., & Watson, A. (2021). Winter air-sea CO_2 fluxes constructed from summer observations of the polar southern ocean suggest weak outgassing. *Journal of Geophysical Research: Oceans*, *126*(5), e2020JC016600. https://doi.org/10.1029/2020JC016600

Mears, C., Lee, T., Ricciardulli, L., Wang, X., & Wentz, F. (2022). RSS Cross-Calibrated Multi-Platform (CCMP) monthly ocean vector wind analysis on 0.25 deg grid, Version 3.0 [Dataset]. In *Remote Sensing Systems (RSS) Air-Sea Essential Climate Variables (AS-ECV). Remote Sensing Systems*. https://doi.org/10.56236/rss-uv1m30

Mongwe, N. P., Chang, N., & Monteiro, P. M. (2016). The seasonal cycle as a mode to diagnose biases in modelled CO_2 fluxes in the Southern Ocean. *Ocean Modelling*, *106*, 90–103. https://doi.org/10.1016/j.ocemod.2016.09.006

Mongwe, N. P., Vichi, M., & Monteiro, P. M. (2018). The seasonal cycle of $p$$CO_2$ and CO_2 fluxes in the Southern Ocean: Diagnosing anomalies in CMIP5 Earth system models. *Biogeosciences*, *15*(9), 2851–2872. https://doi.org/10.5194/bg-15-2851-2018

OBPG, N. (2018). Moderate resolution imaging spectroradiometer (MODIS) Aqua ocean color data [Dataset]. *NASA Ocean Biology Processing Group, Ocean Biology Distributed Active Archive Center. NASA Goddard Space Flight Center*. Retrieved from http://oceancolor.gsfc.nasa.gov/

Prend, C. J., Gray, A. R., Talley, L. D., Gille, S. T., Haumann, F. A., Johnson, K. S., et al. (2022). Indo-Pacific Sector dominates Southern Ocean carbon outgassing. *Global Biogeochemical Cycles*, *36*(7), e2021GB007226. https://doi.org/10.1029/2021GB007226

Remote Sensing Systems. (2022). MW-IR optimum interpolated SST data set. Ver. 5.1. [Dataset]. *PO.DAAC, CA, USA*. https://doi.org/10.5067/GHMWI-4FR51

Ritter, R., Landschützer, P., Gruber, N., Fay, A. R., Iida, Y., Jones, S., et al. (2017). Observation-based trends of the Southern Ocean carbon sink. *Geophysical Research Letters*, *44*(24), 12339–12348. https://doi.org/10.1002/2017GL074837

Rödenbeck, C., Bakker, D. C., Gruber, N., Iida, Y., Jacobson, A. R., Jones, S., et al. (2015). Data-based estimates of the ocean carbon sink variability – First results of the Surface Ocean $p$$CO_2$ Mapping intercomparison (SOCOM). *Biogeosciences*, *12*(23), 7251–7278. https://doi.org/10.5194/bg-12-7251-2015

Saha, K., Zhao, X., Zhang, H. M., Casey, K. S., Zhang, D., Baker-Yeboah, S., et al. (2018). AVHRR Pathfinder version 5.3 level 3 collated (L3C) global 4km sea surface temperature for 1981-Present. [sea_ice_fraction] [Dataset]. *NOAA National Centers for Environmental Information*. https://doi.org/10.7289/v52j68xx

Sutton, A. J., Williams, N. L., & Tilbrook, B. (2021). Constraining Southern Ocean CO_2 flux uncertainty using uncrewed surface vehicle observations. *Geophysical Research Letters*, *48*(3), e2020GL091748. https://doi.org/10.1029/2020GL091748

Takao, S., Nakaoka, S. I., Hashihama, F., Shimada, K., Yoshikawa-Inoue, H., Hirawake, T., et al. (2020). Effects of phytoplankton community composition and productivity on sea surface $p$$CO_2$ variations in the Southern Ocean. *Deep Sea Research Part I: Oceanographic Research Papers*, *160*, 103263. https://doi.org/10.1016/j.dsr.2020.103263

Tu, Z., Le, C., Bai, Y., Jiang, Z., Wu, Y., Ouyang, Z., et al. (2021). Increase in CO_2 uptake capacity in the Arctic Chukchi Sea during summer revealed by satellite-based estimation. *Geophysical Research Letters*, *48*(15), e2021GL093844. https://doi.org/10.1029/2021GL093844

Uchida, T., Balwada, D., Abernathey, R., Prend, C. J., Boss, E., & Gille, S. T. (2019). Southern Ocean phytoplankton blooms observed by biogeochemical floats. *Journal of Geophysical Research: Oceans*, *124*(11), 7328–7343. https://doi.org/10.1029/2019JC015355

Winker, D. M., Vaughan, M. A., Omar, A., Hu, Y., Powell, K. A., Liu, Z., et al. (2009). Overview of the CALIPSO mission and CALIOP data processing algorithms. *Journal of Atmospheric and Oceanic Technology*, *26*(11), 2310–2323. https://doi.org/10.1175/2009JTECHA1281.1

Wu, Y., & Qi, D. (2023). The controversial Southern Ocean air-sea CO_2 flux in the era of autonomous ocean observations. *Science Bulletin*, *68*(21), 2519–2522. https://doi.org/10.1016/j.scib.2023.08.059

Zhang, S., Chen, P., Zhang, Z., & Pan, D. (2022). Carbon air-sea flux in the Arctic Ocean from CALIPSO from 2007 to 2020. *Remote Sensing*, *14*(24), 6196. https://doi.org/10.3390/rs14246196